Video Article

A Coupled Experiment-finite Element Modeling Methodology for Assessing High Strain Rate Mechanical Response of Soft Biomaterials

Rajkumar Prabhu[1], Wilburn R. Whittington[2], Sourav S. Patnaik[1], Yuxiong Mao[2], Mark T. Begonia[1], Lakiesha N. Williams[1], Jun Liao[1], M. F. Horstemeyer[2]

[1]Department of Agricultural and Biological Engineering, Mississippi State University

[2]Center for Advanced Vehicular Systems, Mississippi State University

Correspondence to: Rajkumar Prabhu at praj@cavs.msstate.edu

URL: https://www.jove.com/video/51545
DOI: doi:10.3791/51545

Keywords: Bioengineering, Issue 99, Split-Hopkinson Pressure Bar, High Strain Rate, Finite Element Modeling, Soft Biomaterials, Dynamic Experiments, Internal State Variable Modeling, Brain, Liver, Tendon, Fat

Date Published: 5/18/2015

Citation: Prabhu, R., Whittington, W.R., Patnaik, S.S., Mao, Y., Begonia, M.T., Williams, L.N., Liao, J., Horstemeyer, M.F. A Coupled Experiment-finite Element Modeling Methodology for Assessing High Strain Rate Mechanical Response of Soft Biomaterials. *J. Vis. Exp.* (99), e51545, doi:10.3791/51545 (2015).

Abstract

This study offers a combined experimental and finite element (FE) simulation approach for examining the mechanical behavior of soft biomaterials (*e.g.* brain, liver, tendon, fat, *etc.*) when exposed to high strain rates. This study utilized a Split-Hopkinson Pressure Bar (SHPB) to generate strain rates of 100-1,500 sec^{-1}. The SHPB employed a striker bar consisting of a viscoelastic material (polycarbonate). A sample of the biomaterial was obtained shortly postmortem and prepared for SHPB testing. The specimen was interposed between the incident and transmitted bars, and the pneumatic components of the SHPB were activated to drive the striker bar toward the incident bar. The resulting impact generated a compressive stress wave (*i.e.* incident wave) that traveled through the incident bar. When the compressive stress wave reached the end of the incident bar, a portion continued forward through the sample and transmitted bar (*i.e.* transmitted wave) while another portion reversed through the incident bar as a tensile wave (*i.e.* reflected wave). These waves were measured using strain gages mounted on the incident and transmitted bars. The true stress-strain behavior of the sample was determined from equations based on wave propagation and dynamic force equilibrium. The experimental stress-strain response was three dimensional in nature because the specimen bulged. As such, the hydrostatic stress (first invariant) was used to generate the stress-strain response. In order to extract the uniaxial (one-dimensional) mechanical response of the tissue, an iterative coupled optimization was performed using experimental results and Finite Element Analysis (FEA), which contained an Internal State Variable (ISV) material model used for the tissue. The ISV material model used in the FE simulations of the experimental setup was iteratively calibrated (*i.e.* optimized) to the experimental data such that the experiment and FEA strain gage values and first invariant of stresses were in good agreement.

Video Link

The video component of this article can be found at https://www.jove.com/video/51545/

Introduction

Motivation

The cardinal goal of the coupled Split – Hopkinson Pressure Bar (SHPB) experiment/finite element modeling of soft biomaterials (such as brain, liver, tendon, fat, *etc.*) was to extract their uniaxial mechanical behaviors for further implementation in human body FE simulations under injurious mechanical loads. The human body Finite Element (FE) model consists of a detailed human body mesh and a history dependent multiscale viscoelastic-viscoplastic Internal State Variable (ISV) material model for various human organs. This human body model can be used for a framework to build better standards for injury protection, to design innovative protective gear, and to enable occupant centric vehicular design.

Two modes of high rate injury have been widely observed in human trauma: explosive blast and blunt impact. Blast damage from explosive weaponry is the primary source of traumatic injury (TI) and the leading cause of death on the battlefield[1]. When detonated, these explosives form an outward propagating shock wave that produces large and abrupt accelerations and deformations. The resulting loads pose serious threats to those exposed. Although any part of the anatomy can be injured by shock waves, the prime areas of concern are (1) the lower extremity due to its close proximity to the ground, and (2) the head since injuries can inhibit normal brain function and survival[2,3]. These injuries can be categorized as primary, secondary, or tertiary injuries depending on the type of injury sustained. Because the strength of an explosive is characterized by its weight or size, standoff distance, positive pulse duration, and medium through which it travels, it can be difficult to adequately categorize these injuries[3-6]. Congressional reports indicate that military personnel have suffered nearly 179,000 traumatic injuries due to explosive weaponry and vehicle crashes in Iraq and Afghanistan from 2000 through March 2010[2]. Due to the nature and locations of modern combat, head injuries are a leading concern for both the military and civilians[3].

Aside from combat scenarios, TI has a variety of causes including automotive trauma; rodeo, motorcycle and domestic accidents; and sports injuries. For instance, despite improvements to safety equipment and protocols, mechanically induced traumatic brain injury (TBI) continues to be a leading source of mortality and lifelong morbidity in the U.S. The Center for Disease Control and Prevention (CDC) reports approximately 1.4 million TBI events each year, of which nearly 50,000 are fatal. American football alone accounts for more than 300,000 TBIs each year[7]. Survivors of such injuries are at risk for long-term neurological complications related to sensation, cognition, and communication. At this time there are approximately 5.3 million Americans living with these chronic disadvantages and disabilities. Direct and indirect U.S. medical costs from 2000 to 2010 totaled $60 billion[8]. However, these numbers do not account for non-medical costs and losses, or those incurred by the families and friends supporting TBI patients. Beyond purely economic analysis, TBI-induced disability creates a significant reduction in quality of life that can manifest as a significant burden on families and society.

The need for further understanding of the formation, characterization, and prevention of TI is clear. Biomechanical studies of the underlying mechanisms that cause TI provide insight and opportunity to reduce exposure or improve safety features for those at potential risk for TI. Furthermore, more advancement of the general understanding of TI formation may improve diagnostic methods and criteria, providing medical professionals who treat TI with better means of improving outcomes and saving lives.

A better knowledge of injury mechanisms and a better understanding of the biomechanics of injury development are needed to develop effective protective measures for the human body. Historically, simulations aimed at predicting injuries have been hampered by computational restrictions as well as the fidelity of the anatomical and material models employed. Full body simulations have focused on the overall loads on each body part, but the local stress, strain, and damage in each organ, muscle, bone, *etc.* has not been observed. For example, shoulder moment models use the dimensions of the arm, the load, and the applied angle to search for tabular values that specify whether or not a particular scenario is hazardous. A calculation of that nature is helpful for quick estimates but cannot capture what is happening locally from the hand all the way to the shoulder, especially when damage and injury are intrinsically local. Secondly, FE simulations have been used to capture the local response. The limitation in these efforts has not been FEA itself, but the material models that define each body part's behavior under blast injury loads. Previously employed material models are adapted from simpler materials and have not endeavored to capture the myriad of complex mechanical behaviors exhibited by biological tissues. Therefore, high-fidelity computational models with ISV material models for organs in the human body represent the most realistic way to investigate the physics and biomechanics of TIs, to design innovative protective gear, and to establish better standards for injury metrics.

Background on Split-Hopkinson Pressure Bar (SHPB) and Internal State Variable (ISV) Material Model

Due to ethical issues involved with *in vivo* testing of human organs and the logistical issues associated with broad-scale human cadaveric testing, the current research effort involves mechanical experiments *in vitro* using specimens prepared from organs extracted from animal surrogates (*e.g.*, pig as a most frequently used surrogate). Polymeric SHPB has been the preferred method for *in-vitro* testing soft biomaterials at high strain rates. The relevant deformational behaviors from SHPB testing and corresponding tissue damage-related information from the microstructural features of the tissue are incorporated into our ISV material models for organ mechanical descriptions[9-10]. These material models are then implemented into our virtual human body model to conduct FEA of various injuries. This process enables us to move towards the goal of accurately predicting the physics and nature of an injury for a given organ under diverse mechanical loading conditions (*e.g.* blast-induced, car crash and blunt impact) without the need for further physical experimentation. In order to accurately describe the phenomenological mechanical properties, particularly the higher level strain-rate dependency, of the biomaterials used in the FE simulations of the human body, SHPB experiments were performed on the biomaterials to obtain dynamic mechanical responses at strain rates pertaining to human TIs. An overview of the SHPB setup at the Center for Advanced Vehicular Systems (CAVS), Mississippi State University (MSU) is presented in **Figure 1**.

Previous studies have shown that SHPB testing has three major flaws associated with it[12-18]. The first and most significant one is the material inertial effect, which shows up in the high strain rate mechanical response of a biomaterial specimen as an initial spike. In order to overcome this issue, previous research efforts suggested modifying the geometry of the specimen from cylindrical in shape to cuboidal or annular in shape. The resultant mechanical behaviors from such studies were different from each other because the geometry of the specimen affected the wave propagation, wave interactions, and the mechanical response. This type of modification to the specimen geometry has led to erroneous representations of the mechanical response (multiaxial and non-uniform stress state) of the biomaterial. The second major flaw was the inability to maintain dynamic force equilibrium during a test. Researchers overcame this issue by reducing the sample thickness-to-diameter ratio and/or freezing the tissue prior to testing. While reducing the sample thickness-to-diameter ratio addressed the issue of dynamic force equilibrium, freezing the tissue further complicated the testing procedure as it changed the material properties due to crystallization of water present in the tissue. A number of studies completely abandoned the SHPB to avoid the above mentioned flaws and used shock tubes to obtain the pressure-time response in various animal models (rats, pigs, *etc.*). However, these animal models do not give one-dimensional uniaxial stress-strain behaviors necessary for material models used in FE simulations. The third flaw was the failure of the SHPB to give one dimensional stress-strain results because of the specimen barreling due to the material softness and the amount of water content in the specimen.

Hence, the SHPB presents a viable testing apparatus to garner high strain rate data . For soft materials, however, the SHPB induces bulging that produces a three-dimensional stress state mainly from hydrostatic pressure, yet the one dimensional stress-strain data is desired. We show here how one can still use the SHPB to garner the one-dimensional uniaxial true stress-strain curve for material model calibration; however, the process involved in obtaining the uniaxial true stress-strain curve is complicated. This process includes both the multi-axial experimental data and FE simulation results, and it requires iterative recalibration of the material model constants. The one-dimensional implementation of the ISV material model in MATLAB, also known as material point simulator, requires one-dimensional experimental data for the calibration. So, the ISV material model was optimized using a systematic calibration process. Here, experimental data from SHPB tests was considered in the context of wave theory formulation and dynamic force equilibrium (MSU High Rate Software). In order to account for the viscoelastic dispersion of the polymeric SHPB, viscoelastic dispersion equations, as reported by Zhao *et al.* (2007), were implemented in MSU High Rate Software. The viscoelastic dispersion equations helped in ensuring dynamic force equilibrium while testing. The one-dimensional material point simulator was then adjusted in the context of a couple experiment-FE modeling methodology until the two processes were considered to be appropriately compatible, that is, the data from both were in good agreement. These data were used to adjust the ISV model material constants by comparing the MATLAB material response simulator's (one-dimensional) mechanical response and the SHPB FE model's (one-dimensional) specimen centerline stress. Here the FE model's specimen stress component was along the wave loading direction. Then the three-dimensional behavior of the FE model specimen was calibrated by iteratively performing FE simulations and adjusting ISV constants so that volume-averaged

loading direction stress correlated well with the experimental true stress-strain response. Thus, a process of iterative optimization between the experimental data, FE results, and one-dimensional ISV material model was conducted. **Table 1** gives a summary of the variables of ISV material model (MSU TP Ver. 1.1)[11].

The most important element to this methodology is obtaining the one-dimensional mechanical response of the biomaterial and its material parameters for the ISV material model, which circumvents the SHPB testing issues of the stress-state non-uniformity. It also separates out the initial nonlinear response of the biomaterial arising from inertial effects and renders a mechanical response that is intrinsic to the material. The coupled methodology also showed that a change in the specimen geometry completely changes the Boundary Value Problem (BVP) and the loading direction true stress-strain of the specimen. As such, the above mentioned methodology can be used with any material model (phenomenological or microstructural-based) for calibrating and then simulating high strain rate behaviors of human organs under injurious mechanical loads.

Protocol

NOTE: Ethics Statement: The current work is unique to the institution's research policy, and strictly follows the appropriate bio-safety and Office of Regulatory Compliance (ORC) guidelines.

1. Biomaterial Specimen Procurement

1. Wear personal protective equipment in accordance with standard biosafety protocols of the laboratory and/or institution. Wear closed-toed shoes, long pants, a lab coat, surgical gloves, a protective mask, and safety goggles while handling porcine tissue and testing.
2. Obtain porcine tissue (head, abdomen, or hind leg) of healthy pigs from a local abattoir within 1-2 hr post mortem.
3. Store porcine tissue in biohazard safety bags and then place them in an iced container (~5.56-7.22 °C).
   NOTE: Use a thermometer to check that the temperature in the porcine specimen does not drop below 7.22 °C.
4. Transport porcine tissue to the nearest laboratory (at the College of Veterinary Medicine in Mississippi State University) for dissection.
5. Under the supervision of a veterinarian in the College of Veterinary Medicine, surgically extract porcine organ (brain, liver, muscle, fat, or tendon) and place them in containers filled with phosphate buffered saline (PBS) for temporary storage (pH 7.4).
6. Store the PBS containers in an iced cooler (~5.56-7.22 °C) and immediately transport them to the testing facility for sample preparation and SHPB testing.

2. Biomaterial Sample Preparation

1. Remove the porcine organ from the PBS container and place it on a sterile surface.
2. NOTE: Identify the primary fiber orientation and locations for each test sample. Use a cylindrical die with a 30 mm inner diameter to dissect the test sample from the porcine organ.
3. If the test sample is wedged inside the cylindrical die, inject PBS through the opposite end of the dissection tool to allow the test sample to slide out intact. Place the extracted test sample on a separate area of the sterile surface.
4. Use a scalpel to trim the sample to the prescribed thickness and aspect ratio.
   NOTE: For SHPB testing of porcine samples, the thickness is 10-15 mm while the aspect ratio (thickness/diameter) is 0.33-0.50 (**Figure 2**).
5. Use calipers to measure the thickness and diameter at three different locations.
6. Store all test samples in fresh PBS until the SHPB device is ready for testing.
   NOTE: Ensure that samples are tested within 4 hr after slaughter.
7. Discard samples that are not cylindrical due to incision errors or variations in the cross-section. Place discarded samples in biohazard safety bags. Repeat steps 2.2-2.6 to obtain additional test samples.

3. Split-Hopkinson Pressure Bar Testing

1. Place the striker bar, incident bar, and transmitted bar in the metal stanchions for SHPB testing.
   NOTE: Ensure that bars are free moving to the touch and that their interfaces are aligned with each other. Provide a stopper for transmitted bar for safety.
2. Connect the strain gages adhered to incident and transmitted bars to the signal amplifier. Turn on the signal conditioning amplifiers and the DAQ module computer.
3. Initialize the high speed data capturing software.
4. Verify the live capturing of the signals to see if they lie within the normal range, and nullify the noise signals by clicking the zero icon.
5. Input the trigger level and the data rate (2 MHz).
6. Initialize the software to record once the trigger level has been achieved.
7. Load the striker bar adjacent to the pressure chamber. Fill the pressure chamber to a desired pressure.
   NOTE: The typical pressure range is 5-25 psi.
8. Zero out the laser speed meter by pressing the zero button and set it to read the striker bar velocity by setting the reflector strip on the striker bar behind the laser sensors.
9. Place the sample confinement chamber such that it does not hinder the movement of incident and reflected bar. Place the incident bar in contact with the transmitted bar.
10. For calibration purposes, run a test (without a sample) by turning on trigger switch for the pressure chamber on the striker bar.
11. Once the data is acquired in the computer, save and analyze the SHPB strain gage data (which is discussed in the next section) to ensure that the testing procedure is functioning properly.
12. Place the cylindrical sample between the incident and transmitted bar and then close the sample confinement chamber.
    NOTE: Ensure that no pre-conditioning is performed on the sample.

13. Perform Tasks 3.4-3.7 with the sample placed between the incident and transmitted bar.
    NOTE: Ensure that the sample centerline is the same as the bar centerline. Before proceeding, also check that the sample is not compressed, but remains in the same geometry as previously extracted.
14. After testing is complete, use disposable sanitary wipes to remove sample debris from the incident bar, transmitted bar, and sample confinement chamber. Dispose of all debris and wipes in biohazard safety bags.
15. Sanitize the bars and sample confinement chamber using a 70% ethanol cleaning solution and sanitary wipes.

4. SHPB Data Post-processing

1. Open the "MSU High Rate Software[19]" for analysis of Hopkinson Bar waves.
2. Begin the software by examining the Settings window and choosing the "Tension/Compression" option in the Mode Tab for uniaxial testing. Also, select "2 Gages" in the Gages Tab and click "Continue."
3. In the Main Window, select the Open File 1 Tab, and navigate to the incident wave data from the strain gage record on the incident bar. Select the Open File 2 Tab for importing the transmitted bar strain gage record.
4. Select the Parameters Tab in the Main Window and input the physical parameters of the test setup including: bar dimensions, voltage to strain factors, strain gage positions, and viscoelastic dispersion constants. Click "Continue."
5. Then select the Select Data Tab in the Main Window and use the cursor bars to reduce the dataset to only the amount of data containing the incident, reflected, and transmitted waves. Click "Continue."
6. Then select the Select Waves Tab in the Main Window and use the cursor bars to confine the incident wave in the Incident Wave Graph, the reflected wave in the Reflected Wave Graph, and the transmitted wave in the Transmitted Wave Graph. Click "Continue."
7. After that, select the Correct Tab in the Main Window to allow the software to correct for the viscoelastic dispersion[20-21].
8. Now select the Shift Tab in the Main Window. In the Wave Graph, use the cursor to drag the incident, reflected, and transmitted waves to the same initial position in time by selecting each one individually in the Wave Select Tab. View all of the waves in the Data Graph. Once completed, click "Continue."
9. In the results file, save the load, displacement, position, and velocity, profiles by clicking "Save As."
10. Use conventional methods in Microsoft Excel (or any other spreadsheet software) to calculate true stress and true strain using the specimen dimensions measured before the Hopkinson Bar test.

5. SHPB Finite Element Modeling

1. Using commercial finite element (FE) software, create a FE model of the SHPB setup.
   NOTE: Use the same geometries and material properties.
2. Assign an initial velocity to the FE model of the striker bar to initialize the FE simulation.
   NOTE: The velocity of the striker bar should correspond to that in the SHPB experiment for a particular strain rate[9].
3. Create a FE model of the SHPB setup without a sample placed between the incident and transmitted bars. Run the FE simulation.
   NOTE: The simulated striker bar velocity should correspond to the experimental striker bar velocity under the "no-sample" condition. Assign material properties given in **Table 1** for polymeric bars.
4. Verify if the strain gage measurements (stain versus time) in the experiment and FE simulation are in good agreement.
5. Incorporate the biomaterial sample into the FE model of the SHPB setup. Assign the three-dimensional implementation (in vumat file format[22]) of the ISV material model to the biomaterial sample[11].
6. Perform a mesh refinement study using three different mesh sizes and then analyze the results to determine if the solutions converge.
   NOTE: The mesh size corresponds to the total number of hexahedral and/or tetrahedral elements that comprise the FE model. Select the FE model with the lowest mesh size that converges after further simulations[9].
7. Conduct the two-step FE model calibration. In the first step, upload the experimental data into the one-dimensional implement of the ISV material model.
8. Calibrate the true stress-stain curve of the experiment with the model's true stress-strain curve by adjusting the ISV material model's parameters (see **Table 1**).
   NOTE: Further iterations are needed because the experimental SHPB data is three-dimensional in nature while the material model is one-dimensional.
9. Assign the ISV material constants to the biomaterial sample in the FE model of the SHPB setup.
10. Run the FE simulation with the striker bar velocity and sample deformation strain rate corresponding to the SHPB tests at the same strain rate.
11. Compare the strain gage measurements from experiment and FE simulation for good agreement (strain versus time).
    NOTE: If there is good agreement between the FE simulations and experiment strain gage values, proceed to the second step of the model calibration process. If not, repeat Tasks 5.7-5.11.
12. In the second step of the FE model calibration, run the FE simulation strain gage data SHPB experiment post-processing software, MSU High Rate software[19-21].
    NOTE: If the simulated true stress-strain response compares to the experimental true stress-strain response, then the two-step FE model calibration has been completed. If not, repeat Tasks 5.7-5.12.
13. Perform a volume average of the loading direction (Σ_{33}) stress along the centerline elements of the FE model sample.
    NOTE: If this stress is in good agreement with the stress-strain curve of the one-dimensional ISV material model result, then the results obtained through Tasks 5.7-5.12 are fully calibrated. If not, repeat Tasks 5.7-5.13. The true stress-strain response captured through the one-dimensional implementation of the ISV material model represents the uniaxial true stress-strain response of a biomaterial that was tested in a SHPB setup.

Representative Results

The effectiveness of the coupled methodology is exemplified in **Figure 3**. Here the SHPB experimental stress-strain response for the brain is at a lower stress state (with a peak stress of 0.32 MPa) in comparison to the stress state of the one-dimensional material point simulator (with a peak value of 0.74 MPa), which is akin to the FE sample center line (element) average. This is due to the nature of deformation that soft biomaterials exhibit. Because the strain rates are high, and the wave speed and strength of the biomaterial is low, the inertial and stress wave propagation in the material demand non-uniform deformation. This phenomenon is greatest at the sample edges and least in the center. Because the specimens are cylinders, the center of the specimen cannot displace non-uniform radial expansion unlike the edges. Therefore, after a certain amount of time, the sample centerline can be closely approximated as uniaxial.

Due to the observation of the sample centerline exhibiting uniaxial deformation after some initial "ring-up" time, FEA can then be used to extract the centerline data, which is not possible for the experimental setup to capture. Here the "ring-up" time is the timespan during the initial phase of a SHPB test when stress-state equilibrium is attained. To do this, the virtual FEA strain gages are compared to the experimental strain gages, and the material constants are varied until good agreement is reached. **Table 2** gives the representative material constants for the brain obtained through the coupled SHPB experiment-FE simulation methodology. Further, **Figure 4** shows that the SHPB experimental true stress-strain curve actually measures the first invariant of stress, rather than the uniaxial loading-direction stress-strain behavior. While most other studies[12-18] simply present the experimental results, **Figure 3** shows that such a representation of the mechanical response of a biomaterial would underestimate the uniaxial response, which is relevant for FE modeling simulation of real world boundary value problems (BVPs). Hence, a use of the SHPB experimental result alone would be erroneous if it not coupled with FE-type modeling to assess the uniaxial behavior.

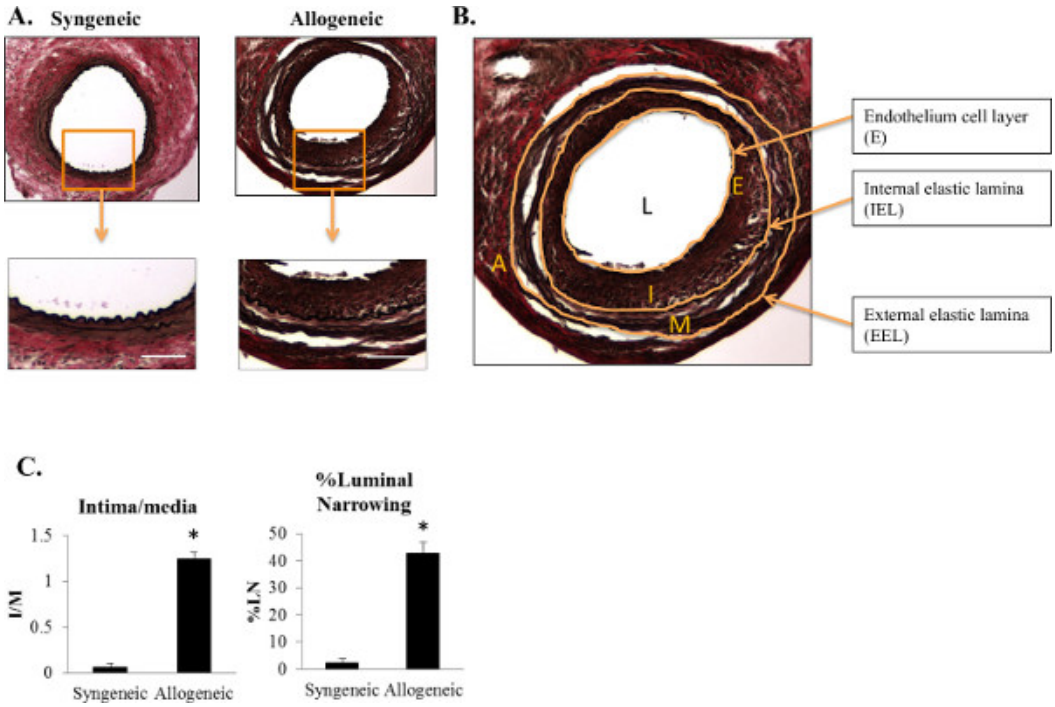

Figure 1: An overview of customized polymer Split-Hopkinson Pressure Bar (SHPB) used for testing porcine brain samples. This figure has been modified from Prabhu *et al.*, 2011[9].

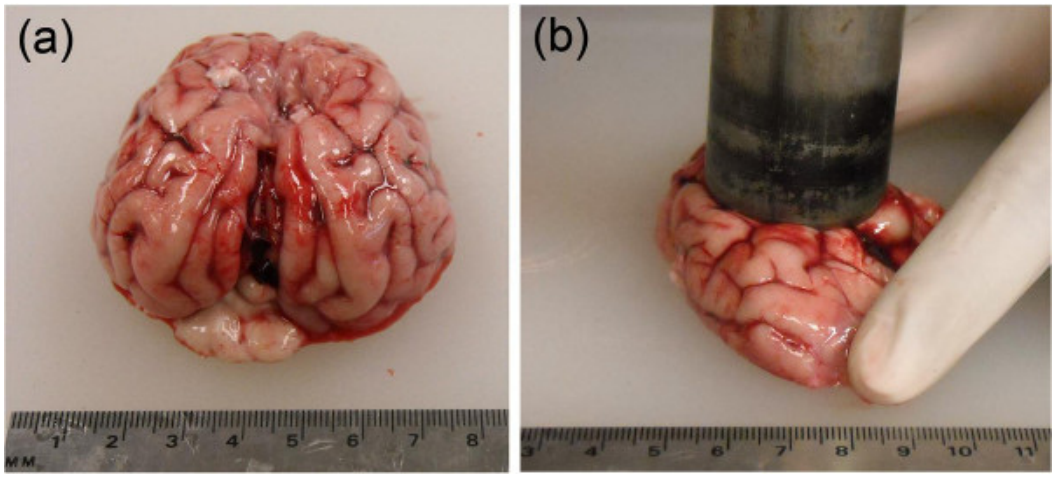

Figure 2: Sample extraction from fresh (< 3 hr post-mortem) from (**a**) porcine brain, and (**b**) sample extraction using a 30 mm inner diameter die in the superior-inferior direction. This figure has been modified from Prabhu *et al.*, 2011[9].

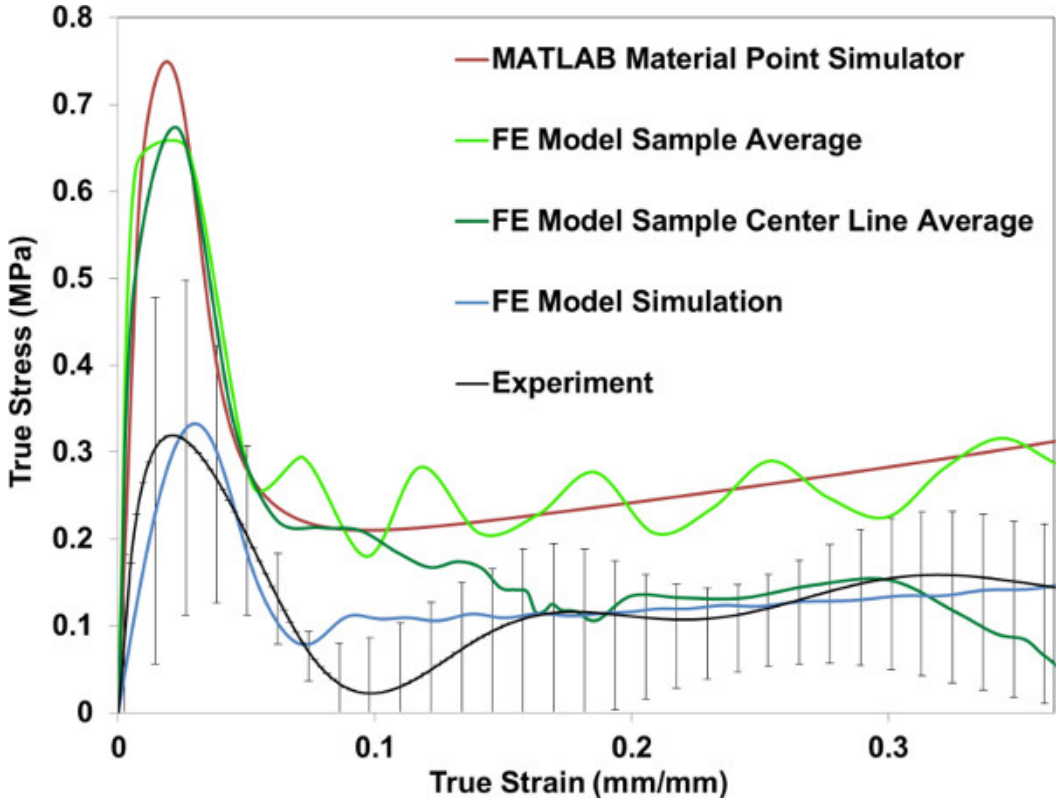

Figure 3: Comparison of Σ_{33} for experiment, MATLAB Fitting Routine (material point simulator), FE specimen average data and FE strain measures through DAVID Viscoelastic, at 750 sec^{-1}. The error bands in the experimental incident/reflected waves represented uncertainty. This figure has been modified from Prabhu *et al.*, 2011[9].

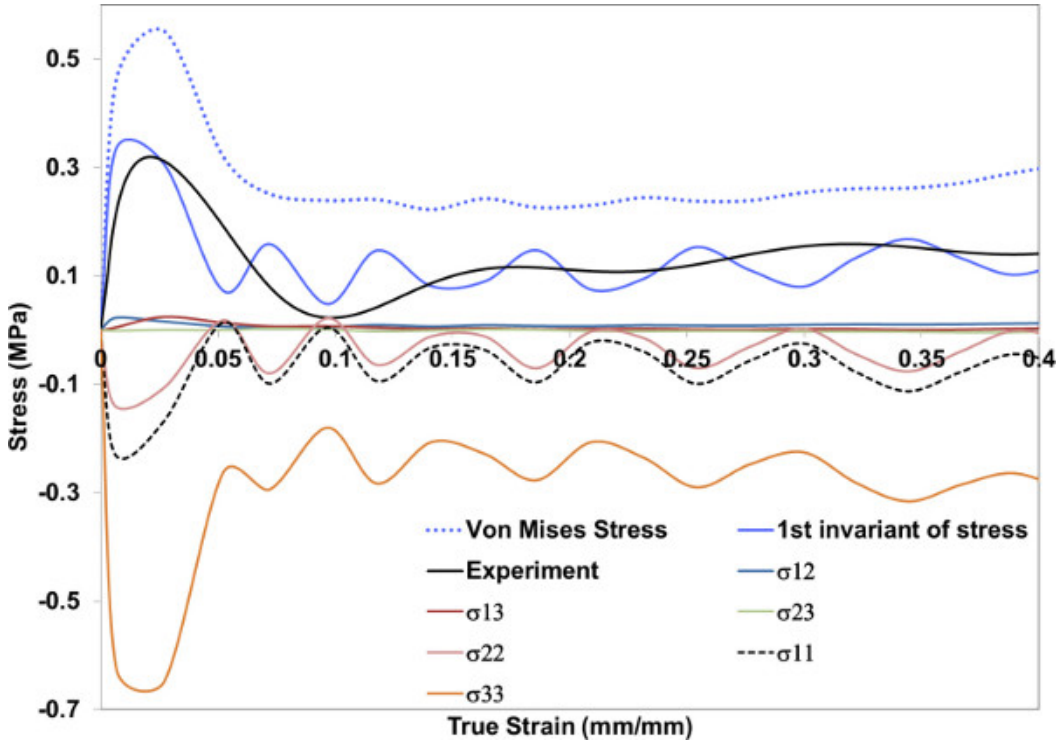

Figure 4: Plots of Finite Element (FE) simulation Σ_{Mises}, Σ_{11}, Σ_{22}, Σ_{33}, Σ_{12}, Σ_{23}, Pressure (First Invariant of Stress) and Σ_{13} and experiment during deformation for cylindrical sample, at 750 sec^{-1}. Here compressive stresses are negative. This figure has been modified from Prabhu *et al.*, 2011[9].

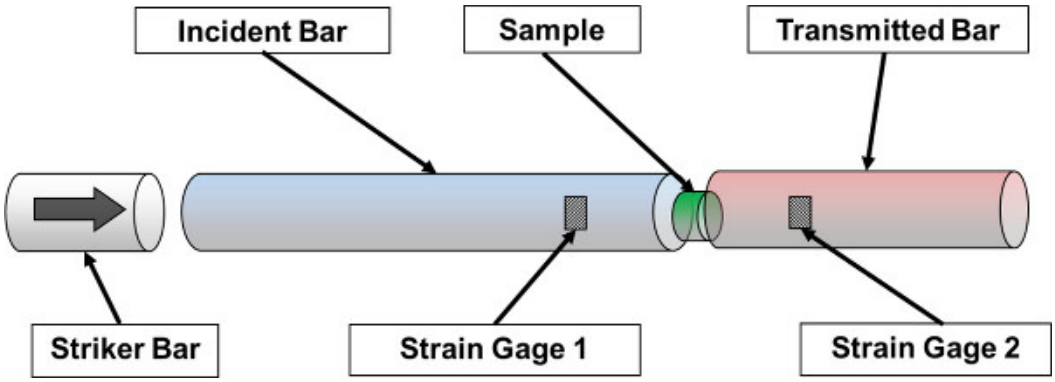

Figure 5: Schematic of the polymeric Split-Hopkinson Pressure Bar (SHPB) setup. This figure has been modified from Prabhu *et al.*, 2011[9].

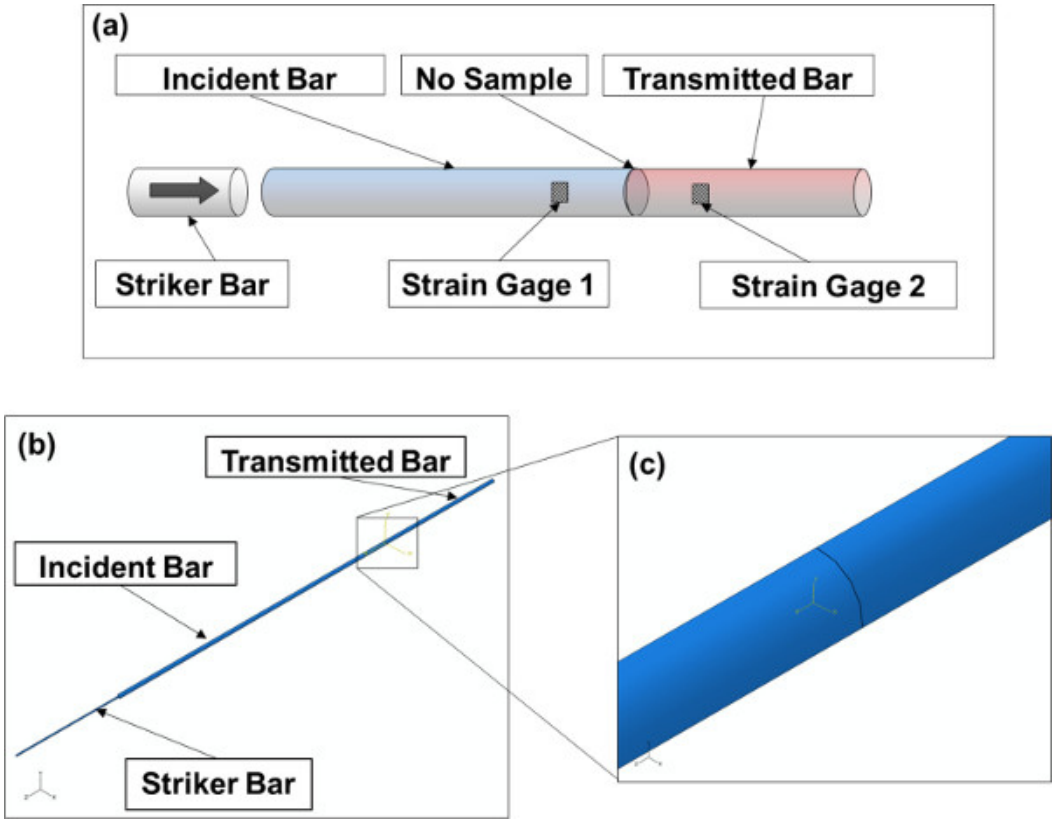

Figure 6: Schematic of the (**a**) experimental set up for SHPB tests and (**b**) FE model simulation along with (**c**) a close-up of the incident-reflected bar interface. This FE model simulation was performed without any sample. FE model damping coefficients α_R and β_R for the simulations were maintained at 3.0 and 1.2.

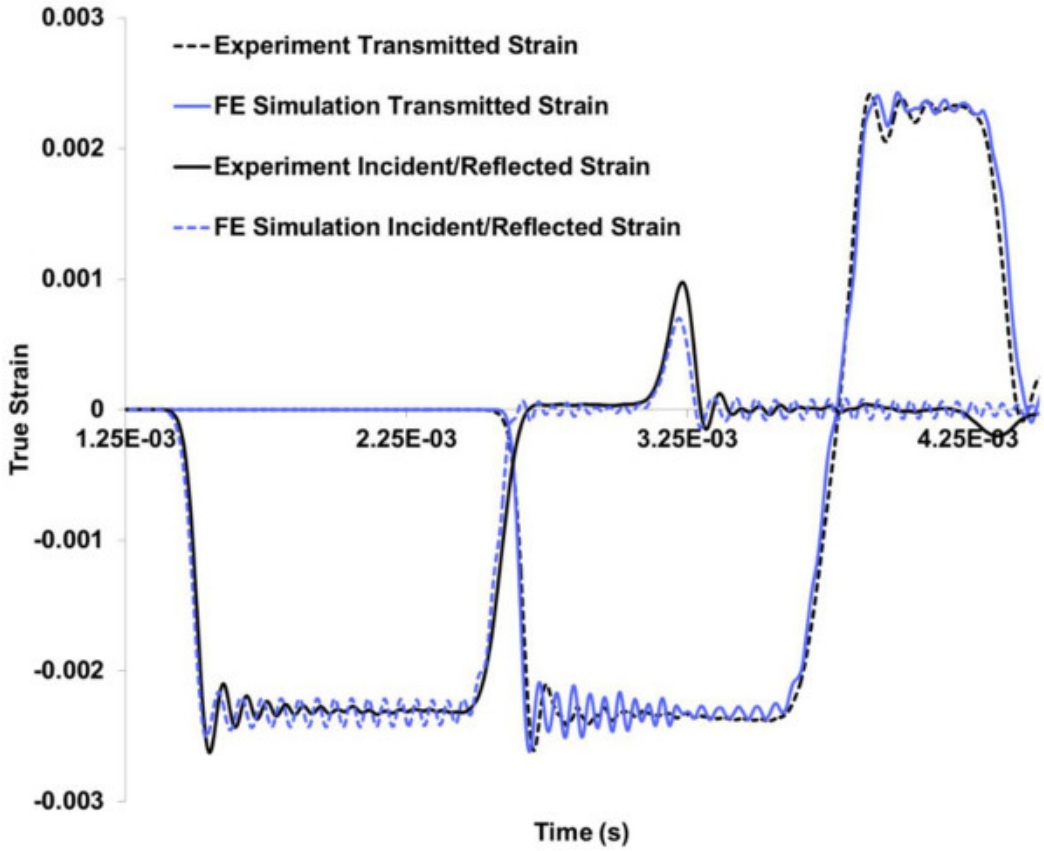

Figure 7: Comparison of experiment and Finite Element (FE) simulation Σ_{33} for porcine brain sample compression, at 6.5 msec^{-1}. FE simulation σ_{33} were calculated by post processing the strain measurements from FE simulation through MSU High Strain Rate software.

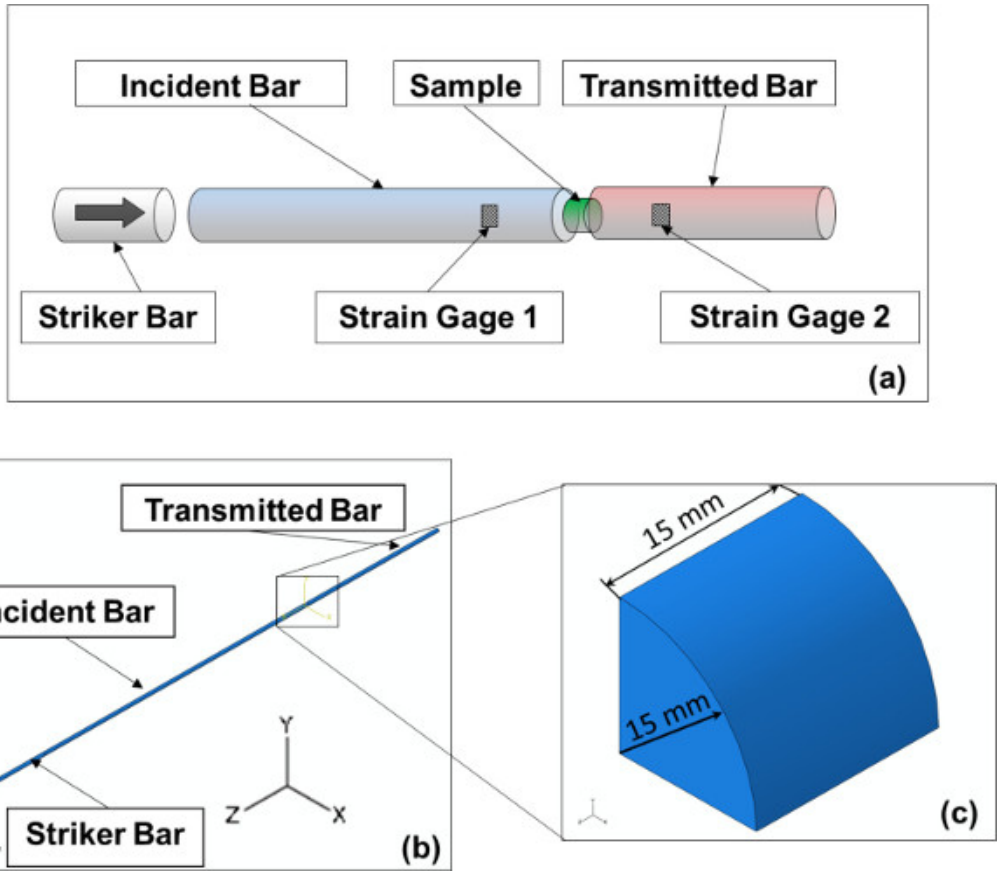

Figure 8: Schematic of (**a**) Finite Element (FE) set up for Split-Hopkinson Pressure Bar (SHPB) tests, (**b**) FE simulation sample dimensions, with a sample, and (**c**) an overview of the SHPB setup with a sample. FE model damping coefficients α_R and β_R for the simulations were maintained at 3.0 and 1.2. This figure has been modified from Prabhu *et al.*, 2011[9].

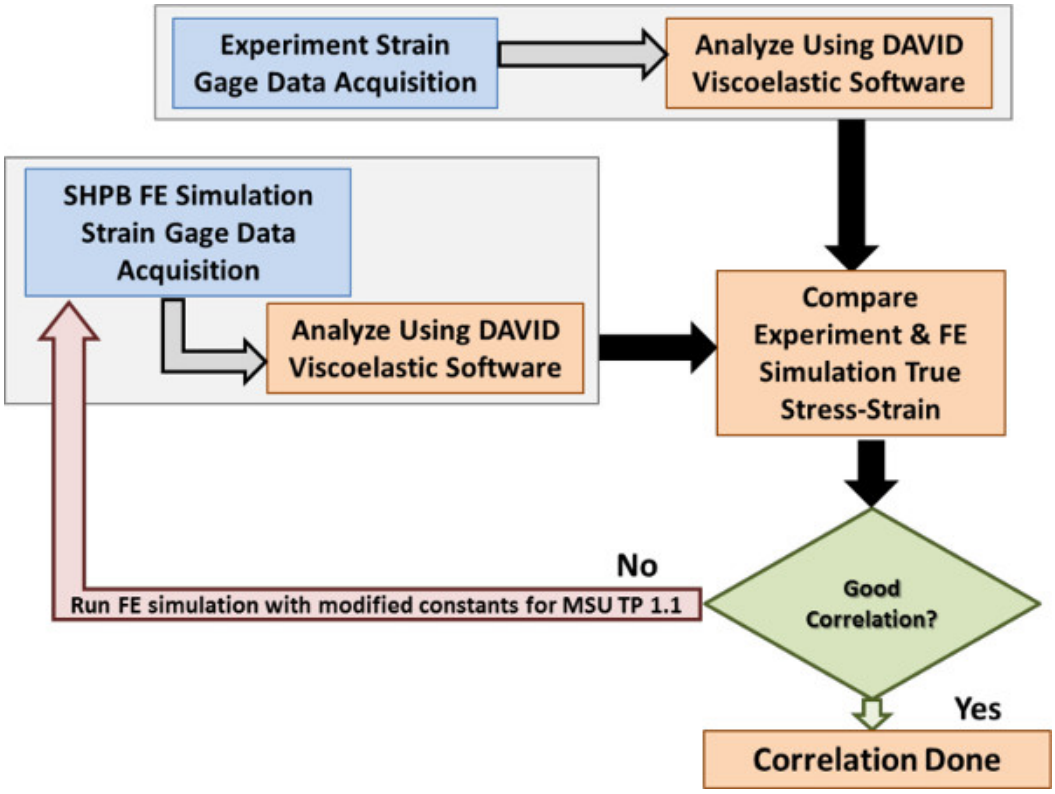

Figure 9: Schematic of the two-fold correlation of the true Stress-strain responses of soft-biological materials for SHPB experiment and FE simulation.

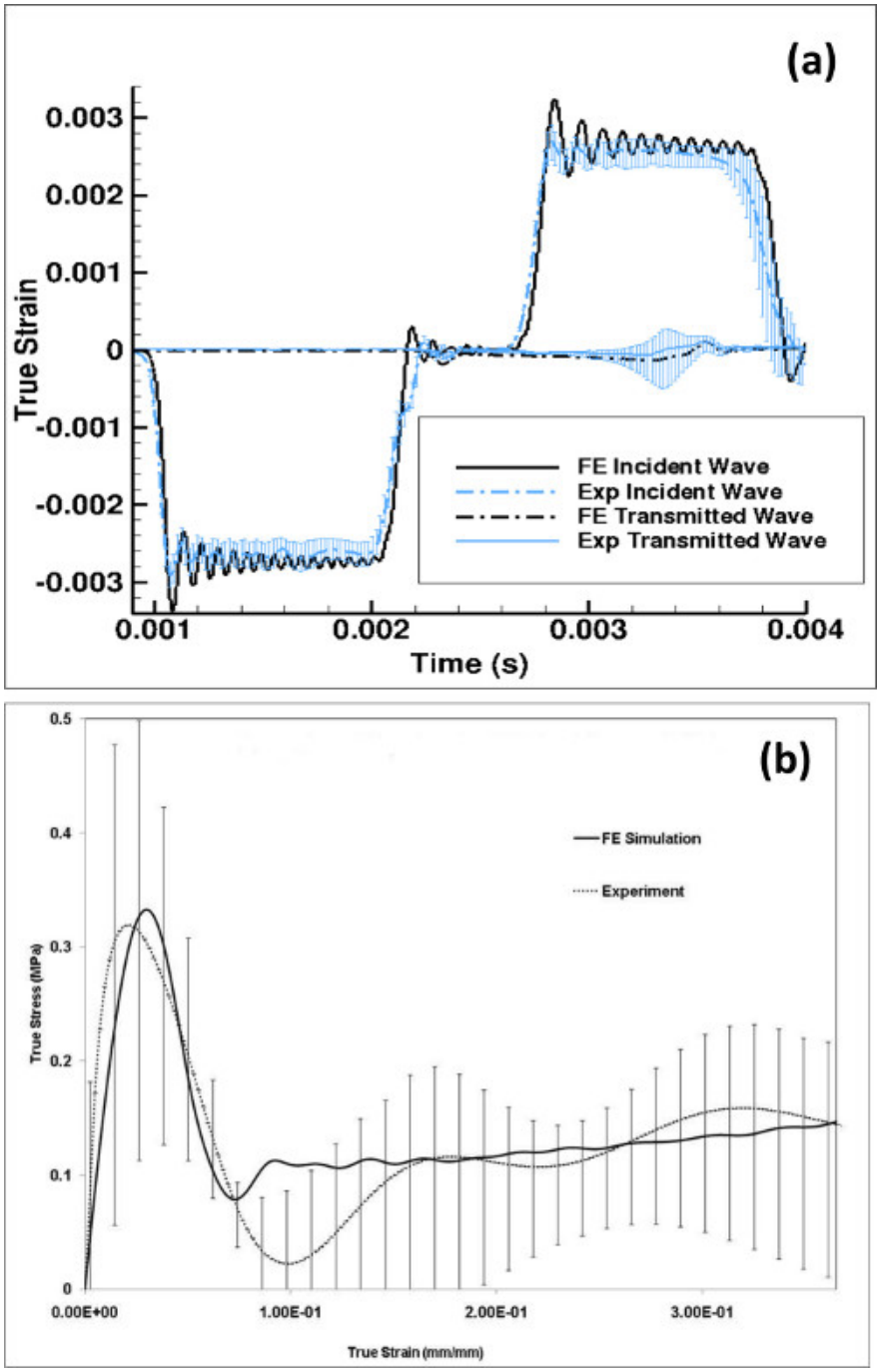

Figure 10. (**a**) Comparison of incident and reflected strain measurements in a Split-Hopkinson Pressure Bar (SHPB), for experiment and Finite Element Analysis (FEA), and (**b**) SHPB experiment and Finite Element (FE) simulation Σ_{33} for porcine brain sample compression at 750 sec^{-1}. FE simulation Σ_{33} were calculated by post processing the strain measurements from FE simulation through DAVID Viscoelastic software. The error bands in the experimental incident/reflected waves represented uncertainty. This figure has been modified from Prabhu *et al.*, 2011[9].

Term/Function	Description
$\Psi = \Psi\left(\bar{C}^{e}, \bar{\xi}_1, \bar{\xi}_2, \bar{E}^{\bar{\beta}}\right)$, where $\bar{C}^{e}$ is the elastic part of the right Cauchy-Green tensor, and $\bar{\xi}_1$, $\bar{\xi}_2$ and $\bar{\mathbf{E}}^{\bar{\beta}}$ are internal strain fields (internal state variables).	Free energy, $\bar{\Psi}$
$\boldsymbol{\sigma} = J^{e-1}\boldsymbol{\tau} = J^{e-1}\mathbf{F}^{e}\bar{\mathbf{S}}\mathbf{F}^{eT}$, where J^{e-1} is the inverse of the determinant of $\mathbf{F}^{e}$. $\mathbf{F}^{e}$ and $\mathbf{F}^{eT}$ are the elastic part of F and the transpose of elastic part of $\mathbf{F}$.	Cauchy Stress, $\boldsymbol{\sigma}$
$\bar{\mathbf{S}} = 2\frac{\partial\hat{\bar{\Psi}}}{\partial\bar{\mathbf{C}}^{e}}$	Second Piola-Kirchhoff stress,
$\boldsymbol{\tau}_1 = \mathbf{R}^{e}\bar{\mathbf{M}}_1\mathbf{R}^{eT}$, where $\mathbf{R}^{e}$ and $\mathbf{R}^{eT}$ are the elastic part of the rotation tensor ($\mathbf{R}$) and the transpose of the elastic part of $\mathbf{R}$.	Kirchhoff Stress (elasto-viscoplas part, $\boldsymbol{\tau}_1$)
$\bar{\mathbf{M}} = 2\mu\mathbf{E}^{e} + \left(K - \frac{2}{3}\mu\right)\mathrm{Tr}(\mathbf{E}^{e})\mathbf{I}$, where μ and K are the elastic shear and bulk moduli modeling the elastic behavior respectively. $\mathbf{E}^{e}$ is the elastic part of the Green-Lagrange strain tensor, and $\bar{\mathbf{I}}$ is the identity matrix.	Elastic Law (Mandel Stress,
$\mathbf{F} = \mathbf{F}^{e}\mathbf{F}^{p}, \mathbf{F}^{e} = \mathbf{R}^{e}\mathbf{U}^{e}, \mathbf{E}^{e} = \ln(\mathbf{U}^{e})$, where $\mathbf{F}^{p}$ is the plastic part of the deformation tensor, and $\mathbf{U}^{e}$ is the right stretch tensor.	Deformation Gradient
$\bar{\kappa}_1 = \frac{\partial\hat{\bar{\Psi}}}{\partial\bar{\xi}_1}$ $\bar{\kappa}_2 = \frac{\partial\hat{\bar{\Psi}}}{\partial\bar{\xi}_2}$, where $\bar{\kappa}_1$ and $\bar{\kappa}_2$ are stress-like thermodynamic conjugates of the $\bar{\xi}_1$ and $\bar{\xi}_2$ respectively.	Stress-like intern state variables Stress-like intern

$$\overline{\boldsymbol{\alpha}} = \frac{\partial \hat{\overline{\psi}}}{\partial \overline{\mathbf{E}}^{\overline{\beta}}},$$ where $\overline{\boldsymbol{\alpha}}$ is a stress-like thermodynamic conjugates of $\overline{\mathbf{E}}^{\overline{\beta}}$.	state variable
$$\dot{\mathbf{F}}^{p} = \overline{\mathbf{D}}^{p}\mathbf{F}^{p},$$ where $\overline{\mathbf{D}}^{p}$ the inelastic rate of deformation. $$\overline{\mathbf{D}}^{p} = \frac{1}{\sqrt{2}}\dot{\gamma}^{p}\overline{\mathbf{N}}^{p} \text{ with } \overline{\mathbf{N}}^{p} = \frac{\mathbf{dev}\overline{\mathbf{M}}_{1}}{\left\|\mathbf{dev}\overline{\mathbf{M}}_{1}\right\|},$$ where $\dot{\bar{\gamma}}^{p}$ is the viscous shear strain rate given by the following equation: $$\dot{\bar{\gamma}}^{p} = \dot{\bar{\gamma}}_{0}^{p}\left[\sinh\left(\frac{\left\langle \bar{\tau} - \left(\bar{\kappa}_{1} + \bar{\kappa}_{2} + \alpha_{p}\bar{\pi}\right)\right\rangle}{Y}\right)\right]^{m}$$ $$\text{with } \bar{\tau} = \frac{1}{\sqrt{2}}\left\|\overline{\mathbf{DEV}}\left(\overline{\mathbf{M}} - \overline{\boldsymbol{\alpha}}\right)\right\| \text{ and } \bar{\pi} = -\frac{1}{3}\overline{\mathrm{Tr}}\left(\overline{\mathbf{M}}\right),$$ where $\bar{\tau} = (1/\sqrt{2})\|\overline{\mathbf{DEV}}(\overline{\mathbf{M}} - \overline{\boldsymbol{\alpha}})\|$ is an equivalent shear stress term and $\bar{\pi} = (1/3)\overline{\mathrm{Tr}}(\overline{\mathbf{M}})$ is the effective pressure term, $\dot{\bar{\gamma}}_{0}^{p}$ is a reference strain rate, m is a strain rate sensitivity parameter, and α_p is a pressure sensitivity parameter and Y is the yield criterion.	Flow rule Equivalent plasti shear strain-rate
$$\dot{\bar{\xi}}_{1} = h_{0}\left(1 - \frac{\bar{\xi}_{1}}{\bar{\xi}^{*}}\right)\dot{\bar{\gamma}}^{p} \quad \dot{\bar{\xi}}^{*} = g_{0}\left(1 - \frac{\bar{\xi}^{*}}{\bar{\xi}_{sat}^{*}}\right)\dot{\bar{\gamma}}^{p},$$ where ξ^* represents an evolving strain threshold or criterion that the macromolecular chains have to overcome to slip. h_0 and g_0 are hardening moduli, and ξ_{sat}^{*} is the saturation value of ξ^*.	Polymer chain resistance to plas flow
$$\dot{\bar{\xi}}_{2} = h_{1}\left(\bar{\lambda}^{p} - 1\right)\left(1 - \frac{\bar{\xi}_{2}}{\bar{\xi}_{2sat}}\right)\dot{\bar{\gamma}}^{p} \text{ with } \bar{\lambda}^{p} = \frac{1}{\sqrt{3}}\sqrt{\overline{\mathrm{Tr}}\left(\overline{\mathbf{B}}^{p}\right)} \text{ and } \overline{\mathbf{B}}^{p} = \mathbf{F}^{p}\mathbf{F}^{pT}$$ where h_1 is an hardening modulus, and ξ_{2sat} is the saturation value of ξ_2.	Polymer chain crystallization at large strain
$$\dot{\overline{\boldsymbol{\beta}}} = R_{s_1}\left(\overline{\mathbf{D}}^{p}\overline{\boldsymbol{\beta}} + \overline{\boldsymbol{\beta}}\overline{\mathbf{D}}^{p}\right) \text{ and } \overline{\boldsymbol{\beta}}(\mathbf{X},0) = \mathbf{I}$$	Evolution equati of stretch-like tensor $\overline{\boldsymbol{\beta}}$

Table 1: Summary of the variables and model Equations for MSU TP 1.1. This table has been modified from Prabhu *et al.*, 2011[9] and Bouvard *et al.*, 2010[11].

Model Constants	Values
μ (MPa)	25.00
K (MPa)	12492.00
γ_{vo} (sec^{-1})	100000.00
m	1.00
Y_o (MPa)	8.20
α_p	0
λ_L	5.00
μ_R	0.05
R_{s1}	1.40
h_o	47.21
x^o_1	0.75
x^*_{sat}	0.01
x^*_o	1.20
g_o	0.30
$C\kappa_1$ (MPa)	0.40
h_1	0
e^o_{s2}	0
e^{sat}_{s2}	0.40
$C\kappa_2$ (MPa)	0

Table 2: Values of material constants for brain material using MSU TP 1.1 Viscoplasticity model. This table has been modified from Prabhu *et al.*, 2011[9].

	Striker Bar	Incident bar	Transmitted Bar
Material	1-1/2"Polycarbonate (PC) rod*	1-1/2"Polycarbonate (PC) rod*	1-1/2"Polycarbonate (PC) rod*
Density (kg/m^3)	1.220×10^3	1.220×10^3	1.220×10^3
Diameter (m)	1.285×10^{-3}	3.810×10^{-2}	3.810×10^{-3}
Length (m)	7.620×10^{-1}	2.438	1.219

*McMaster-Carr™ 1-1/2" rod (McMaster-Carr™, Chicago, IL, USA).

Table 3: Dimensions and material properties of the polymeric bars used in Split-Hopkinson Pressure Bar (SHPB) setup. This table has been modified from Prabhu *et al.*, 2011[9].

Discussion

The reported methodology that couples the SHPB experiment and FE modeling of the SHPB offers a novel and unique technique to assess the uniaxial true stress-strain response of a biomaterial at high strain rates. In order to procure mechanical properties intrinsic to the native tissue, care must be taken to keep the biomaterial specimen between 5.56–7.22 °C before SHPB testing. If the specimen is cooled below 5.56 °C, water present in the tissue starts to crystalize into ice and subsequently changes the tissue's mechanical properties. While other researchers[15-18] have frozen the sample for preservation purposes from mechanical degradation, the results obtained thereof from SHPB testing yield considerably different mechanical responses. Further, a report by Van Ee and Myers[23] showed that soft biomaterials tested within 5 hours post mortem gave the best experimental results. Additionally, the PBS solution was chosen to store biomaterial specimens and cylindrical samples because its osmolarity and ion concentration are similar to biological fluids[9].

Based on the work by Gray and Blumenthal[24] in the ASM Handbook on high strain rate testing of soft materials, an optimum sample aspect ratio, or ratio of sample thickness to diameter, was determined to be 0.5 or less depending on the type of biomaterial being tested (porcine brain, liver, tendon or fat). Gray and Blumenthal[24] observed in their study that samples with an aspect ratio greater than 0.5 did not accommodate the dynamic force equilibrium during a SHPB test. Sample extraction began by using a stainless steel die to dissect the biomaterial in the superior-inferior direction to create a long, cylindrical piece of biomaterial. A surgical scalpel was then used to cut 15 mm thick samples from

the long cylinder, yielding multiple cylindrical test samples (**Figure 2**). The sample closest to the superior side of the specimen was normally characterized with the organ's surface contour (superior or upper surface). For instance, when a brain specimen was dissected the brain sulci and gyri characterized the upper surface. Here care was taken to ensure the flatness of the surface, which was obtained by incising the "uneven" superior surface with a surgical scalpel. In general, samples' thickness variations were less than 0.5 mm, which came to 3% of the average sample thickness. The samples were assumed to have uniform thickness as the variation in thickness was less than 3%. Procurement of biomaterials was completed in under 1 hr, and all SHPB tests were performed in under 4 hours after sacrifice.

The SHPB stress-wave data was recorded through a series of strain gages affixed to the incident and transmitted bar. The test setup described here used polymeric bars in lieu of the traditional metal bars, as these have been observed to produce a lower noise floor[25]. A detailed list of the SHPB polymeric bars' materials and dimensions are given in **Table 3.** Prior to analyzing the biomaterial, the SHPB apparatus was calibrated and verified using a series of "no-sample" experiments. These experiments served to verify the proper functioning of the incident and transmitted bar strain gages and to evaluate any noise or interference introduced by the metal casings, strain gages, or DAQ system. The SHPB functioned by releasing compressed nitrogen via the pneumatic actuator to rapidly accelerate the striker bar. The striker bar then impacted the incident bar, and the compressive stress wave created by this impact propagated through the incident bar. When the stress wave reached the end of the incident bar, the associated kinetic energy was split with a portion manifested as a reflected tensile stress wave in the incident bar, and the remaining energy manifested as a compressive stress wave transferred to the subsequent media. In the specimen test setup, the compressive wave traveled into the specimen and then into the transmitted bar while the "no-sample" test allowed the compressive wave to move directly from the incident to the transmitted bar. The stress waves recorded here produced different pressures within the incident bar, sample, and transmitted bar, and these pressures served as the boundary conditions for simulating the range of strain rates observed in SHPB experiments.

FE modeling of SHPB tests required two-stages in a manner similar to the experimental apparatus verification. The FE model of the apparatus itself was calibrated for the "no-sample" case (**Figure 6**) in which all three polymeric bars were assigned elastic material properties with a Young's Modulus of 2,391 MPa and Poisson's ratio of 0.36. In **Figure 6**, the negative z-axis denotes the direction of loading with σ_{33} denoting the corresponding compressive stress. This calibration ensured that the polymeric bars possessed suitable material properties and that strain gage measurements in the FE model were comparable to results from the "no-sample" case (**Figure 7**). After the FE model of the apparatus was validated, the biomaterial sample was added and the "sample" test case was subjected to a calibration, verification, and validation process (**Figure 7**). The appropriateness of the element size in our mesh (FE model verification) was tested using a mesh convergence approach. Meshes of the same geometry were constructed with a series of increasingly smaller elements; the meshes ranged in size from 4,703 to 3,111,000 total elements. This convergence study indicated that meshes of 12,000 elements or more provided similar results, thus representing the minimum threshold of convergence. This study also used a material model (MSU TP Ver. 1.1) capable of describing the complex material behaviors exhibited by biomaterials in general. Here, the material model captures the viscoelastic-viscoplastic responses of amorphous materials along with history effects and strain rate dependency, which is currently being used to describe the material responses of brain[9] and liver[26]. The elastic and inelastic responses were characterized using a set of constitutive relationships summarized in **Table 1**. These equations allowed the model to express and reconcile short-term behavior associated with dynamic or instantaneous material response, as well as long-term behavior associated with steady-state material responses. The model also provides the capability to include history effects related to changes in the biomaterial microstructure through the use of ISVs.

The FE model was calibrated through a series of steps (**Figure 9**). SHPB experimental data was used to calibrate the ISV constitutive model using a material point simulator. Then, the experimental and FEA strain gage data were both examined until good agreement was confirmed (**Figure 9**). Next, the strain gage measurements from SHPB tests and FE simulations were compared (**Figure 10**). Correlations were achieved in determining strain gage measurements from the SHPB system and the mechanical response of the sample. It should be pointed out that during calibration the material point simulator yielded a one-dimensional stress state while both SHPB experiments and FE simulations yielded a three-dimensional stress state. The varying stress states produced corresponding differences in σ_{33} (**Figure 10**). The material model constants were optimized until the σ_{33} from SHPB tests matched the σ_{33} from FE simulations. Here the process of optimization was carried out iteratively until the experimental and FE strain gage results were in good agreement along with the three-dimensional stress states obtained by processing the experimental and FEA strain gage data through the MSU high rate software. Additionally, the iterative optimization was also conducted such that the one-dimensional material point simulator and the one-dimensional FE specimen centerline σ_{33} were also in good agreement.

The resulting one-dimensional true stress-strain behavior obtained through the material point simulator then represents the equivalent uniaxial true stress-strain response for a biomaterial obtained through SHPB tests at high strain rates. In summary, the above mentioned methodology gives an effective way to extract the uniaxial experimental result by using the FE simulation tool. The coupled SHPB experiment-FE simulation also alleviated ambiguities concerning theories on inertial effects by showing that much of the stress-strain response was intrinsic to the biomaterial. Finally, the effects of sample geometry modifications (cylindrical versus annular) were observed to have minimal effect in negating the so called inertial effect, which drove the "initial spike." The usage of this methodology is limited to soft biomaterials and is time consuming. Additionally, the coupling of the SHPB experiment and SHPB FE model with an ISV material model is complex. However, the primary advantage of this methodology is that the resulting material constants and the ISV model can be used for simulating diverse mechanical injury scenarios.

Disclosures

The authors hereby declare that there are no conflict of interests with all material related to this publication.

Acknowledgements

The authors would like to recognize the Center for Advanced Vehicular Systems (CAVS) and the Agricultural and Biological Engineering Department at Mississippi State University for supporting this work. This material is based upon work supported by the U.S. Army TACOM Life Cycle Command under Contract No. W56HZV-08-C-0236, through a subcontract with Mississippi State University, and was performed for the Simulation Based Reliability and Safety (SimBRS) research program. Also, this material is based upon work supported by the National Nuclear

Security Administration, (Department of Energy) under award number [DE-FC26-06NT42755]. Finally, the authors would like to thank Mr. David Adams, Mr. Michael McCollum and Ms. Erin Colebeck for their effort in this research.

References

1. Champion, H. R., Holcomb, J. B., Young, L. A. Injuries from explosions: physics, biophysics, pathology, and required research focus. *J Trauma.* **66**, (5), 1468-1477 (2009).
2. Aubry, M. Summary and agreement statement of the First International Conference on Concussion in Sport, Vienna 2001. Recommendations for the improvement of safety and health of athletes who may suffer concussive injuries. *Br J Sports Med.* **36**, (1), 6-10 (2002).
3. Born, C. T. Blast trauma: the fourth weapon of mass destruction. *Scand J Surg.* **94**, (4), 279-285 (2005).
4. Cullis, I. G. Blast waves and how they interact with structures. *J R Army Med Corps.* **147**, 16-26 (2001).
5. Ngo, T., Mendis, P., Gupta, A., Ramsay, J. Blast Loading and Blast Effects on Structures–An Overview. *Electronic Journal of Structural Engineering.* **7**, 76-91 (2007).
6. Usmani, Z. Intelligent Agents in Extreme Conditions – Modeling and Simulation of Suicide Bombing for Risk Assessment. *Web Intelligence and Intelligent Agents.* (2010).
7. Guskiewicz, K. M. Cumulative effects associated with recurrent concussion in collegiate football players the NCAA Concussion Study. *JAMA.* **290**, (19), 2549-2555 (2003).
8. Finkelstein, E., Corso, P., Miller, T. *The Incidence and Economic Burden of Injuries in the United States.* Oxford University Press New York (NY) (2006).
9. Prabhu, R. Coupled experiment/finite element analysis on the mechanical response of porcine brain under high strain rates. *JMech Behav Biomed Mater.* **4**, (7), 1067-1080 (2011).
10. Horstemeyer, M. F. *Integrated Computational Materials Engineering (ICME): Using Multiscale Modeling to Invigorate Engineering Design with Science*. Wiley Press (2012).
11. Bouvard, J. L. A general inelastic internal state variable model for amorphous glassy polymers. *Acta Mechanica.* **213**, 1-2 (2010).
12. Kenner, V. H., Goldsmith, W. Impact on a simple physical model of the head. *J Biomech.* **6**, (1), 1-11 (1973).
13. Khalil, T. B., Viano, D. C., Smith, D. L. Experimental analysis of the vibrational characteristics of the human skull. *J. Sound Vib.* **63**, (3), 351-376 (1979).
14. Pervin, F., Chen, W. W. Dynamic mechanical response of bovine gray matter and white matter brain tissues under compression. *J Biomech.* **42**, (6), 731-735 (2009).
15. Prevost, T. P., Balakrishnan, A., Suresh, S., Socrate, S. Biomechnics of brain tissue. *Acta Biomater.* **7**, (1), 83-95 (2011).
16. Saraf, H., Ramesh, K. T., Lennon, A. M., Merkle, A. C., Roberts, J. C. Mechanical properties of soft human tissues under dynamic loading.J. *J Biomech.* **40**, (9), 1960-1967 (2007).
17. Van Sligtenhorst, C., Cronin, D. S., Wayne Brodland, G. High strain rate compressive properties of bovine muscle tissue determined using a split Hopkinson bar apparatus. *J Biomech.* **39**, (10), 1852-1858 (2006).
18. Song, B., Chen, W., Ge, Y., Weerasooriya, Y. Dynamic and quasi-static compressive response of porcine muscle. *J Biomech.* **40**, (13), 2999-3005 (2007).
19. *MSU JHBT Data Processing and MSU High Rate Software Manual.* Available from: https://icme.hpc.msstate.edu/mediawiki/index.php/File:MSU_JHBT_Data_Processing_and_MSU_High_Rate_Software_Manual.zip (2014).
20. Zhao, H., Gary, G. On the use of SHPB techniques to determine the dynamic behavior of materials in the range of small strains. *Int J Solids Struct.* **33**, (23), 3363-3375 (1996).
21. Zhao, H., Gary, G., Klepaczko, J. R. On the use of a viscoelastic split hopkinson pressure bar. *Int J Impact Eng.* **19**, (4), 319-330 (1997).
22. *MSU TP Ver 1.1.*. Available from: https://icme.hpc.msstate.edu/mediawiki/index.php/File:MSU_TP_Ver_1.1.zip (2014).
23. Gray, G. T., Blumenthal, W. R. *ASM Handbook, Mechanical Testing and Evaluation*. **8**, 488-496 ASM International (2000).
24. Dharan, C. K. H., Hauser, F. E. Determination of stress-strain characteristics at very high strain rates. *Exp. Mech.* **10**, (9), 370-376 (1970).
25. Chen, J., Priddy, L. B., Prabhu, R., Marin, E. B., Horstemeyer, M. F., Williams, L. N., Liao, J. Traumatic Injury: Mechanical Response of Porcine Liver Tissue under High Strain Rate Compression Testing. *Proceedings of the ASME 2009 Summer Bioengineering Conference (SBC2009).* Resort at Squaw Creek Lake Tahoe, CA, USA (2009).

